VIP

Ultrafast NMR T_1 Relaxation Measurements: Probing Molecular Properties in Real Time

Pieter E. S. Smith, Kevin J. Donovan, Or Szekely, Maria Baias, and Lucio Frydman*[a]

The longitudinal relaxation properties of NMR active nuclei carry useful information about the site-specific chemical environments and about the mobility of molecular fragments. Molecular mobility is in turn a key parameter reporting both on stable properties, such as size, as well as on dynamic ones, such as transient interactions and irreversible aggregation. In order to fully investigate the latter, a fast sampling of the relaxation parameters of transiently formed molecular species may be needed. Nevertheless, the acquisition of longitudinal relaxation data is typically slow, being limited by the requirement that the time for which the nucleus relaxes be varied incrementally until a complete build-up curve is generated. Recently, a number of single-shot-inversion-recovery methods have been developed capable of alleviating this need; still, these may be challenged by either spectral resolution restrictions or when coping with very fast relaxing nuclei. Here, we present a new experiment to measure the T_1s of multiple nuclear spins that experience fast longitudinal relaxation, while retaining full high-resolution chemical shift information. Good agreement is observed between T_1s measured with conventional means and T_1s measured using the new technique. The method is applied to the real-time investigation of the reaction between D-xylose and sodium borate, which is in turn elucidated with the aid of ancillary ultrafast and conventional 2D TOCSY measurements.

1. Introduction

Nuclear magnetic resonance (NMR) relaxation parameters are useful in a variety of contexts, and in particular as probes of molecular dynamics occurring on a wide range of time-scales—from pico- to microseconds. These dynamics can in turn reveal unique information about the conformation and functioning of molecules, including vistas into how motions can enable enzymatic or biological function.[1,2] Moreover, fast motions are, in themselves, important in the activity of a variety of biomolecules.[3,4] Longitudinal relaxation time (T_1) measurements are an important probe of these faster timescale motions.[5,6] This method is complementary to pulsed field gradient spin echo (PGSE) techniques, enabling the study of overall molecular sizes and local dynamics by the distinct T_1s values displayed by shift-resolved sites.[7–9] Moreover, when applied to monitor unidirectional dynamics by rapid mixing of liquid samples, T_1 measurements are free from turbulent-motion effects that are often encountered and may jeopardize real-time NMR studies based on PGSE.

T_1 relaxation measurements are usually accomplished using the inversion-recovery (IR) method. In this experiment, spins are inverted by a π pulse, are allowed to relax for a period Δ_{IR}, and are then brought into the transverse plane for detection by a π/2 pulse. Importantly, this experiment requires incrementally varying Δ_{IR}, which incurs a time cost. Traditional IR methods are therefore not suitable for studying in real-time the changes occurring in a molecule's structure or flexibility as it interacts with its environment. These changes in flexibility are important in the thermodynamics of molecular interactions, reporting on the essential entropic contribution of changes in free energies.[10–18] This was realized early on in the progress of NMR,[19] and is routinely exploited in instances which, similar to magnetic resonance imaging, have no need to include a high-resolution chemical shift dimension.[20–22] A number of recent studies have been aimed at developing fast IR experiments, which can also describe site-specific chemical shifts. Bhattacharya et al. have developed a single-scan-IR experiment,[23] but which is ill suited to measuring short T_1s. Other methods for measuring site-resolved T_1s in a single scan, such as the small flip-angle technique proposed by Kaptein et al.[24] and demonstrated in hyperpolarized samples by Day et al.,[25] are again more suited to measuring long T_1s. Although this technique has the advantage of avoiding the sources of error associated with the use of slice-selective pulses or the spatial encoding of relaxation parameters, it requires accurate calibration of pulse flip angles. Loening et al. have also developed alternatives to measure T_1 relaxation in a single shot,[26] but once again they are challenged by short relaxation times or by spectral resolution restrictions.

To address the need for a single-shot longitudinal-relaxation measurement capable of handling short relaxation times without suffering from resolution restrictions, we propose a new pulse sequence where T_1 relaxation is encoded spatially and the sample is imaged using a detection scheme akin to echo planar spectroscopic imaging (EPSI).[27] The new IR sequence,
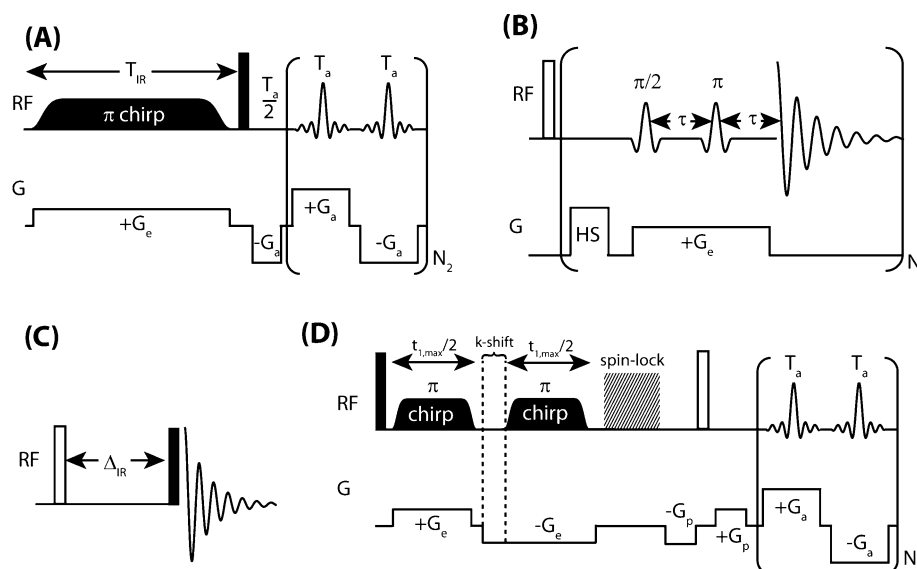
[a] Dr. P. E. S. Smith, Dr. K. J. Donovan, O. Szekely, Dr. M. Baias, Prof. Dr. L. Frydman
Department of Chemical Physics
Weizmann Institute of Science
Rehovot 76100 (Israel)
E-mail: lucio.frydman@weizmann.ac.il

which falls within the domain of ultrafast methods, is applied to study the D-xylose and borate reaction, a process that is relevant to the design of affinity ligands for the separation of carbohydrates and to the construction of saccharide sensors.[28–31] A comparison is made between the new ultrafast IR (UF-IR) method and the multiple-acquisitions IR (MA-IR) experiment of Loening et al;[26] it is shown that each sequence functions optimally in its own niche—ultrafast sequences when T_1s are short and MA-IR when T_1s are longer—thus providing an optimal complement for each other. Additional insight into the interaction between D-xylose and borate was garnered by monitoring in real time their reaction by ultrafast TOCSY,[32] which demonstrated how single-shot 2D methods probing molecular flexibility and structure in real time can function synergistically in dynamic real-time investigations.

Figure 1. Pulse sequences employed in this study; filled rectangles indicate π/2 pulses and empty ones indicate π pulses. A) UF-IR experiment. A linear frequency swept (chirped) inversion pulse is applied with a gradient. Spins at one end of the sample—e.g. at its bottom—that are on resonance at the start of the frequency sweep are inverted first and experience longitudinal relaxation for a longer period than spins that are on resonance later and are therefore inverted later. After T_1 relaxation is spatially encoded with a 1 s WURST-40 π chirp pulse, the precession frequencies of the spins are monitored using an EPSI-type procedure. B) MA-IR technique.[26] A hard π pulse inverts all the sample magnetization, and spins from single slices throughout the sample are rendered observable by the combined effect of a gradient and frequency selective π/2 and π pulses. C) Conventional inversion-recovery experiment. D) Ultrafast 2D TOCSY experiment; a DIPSI-2 sequence was used for spin-lock during the mixing period.[32]

Materials and Methods

Pulse-sequencing considerations: The UF-IR approach utilized here to measure multiple sites' longitudinal relaxation recoveries in a single scan, begins with the simultaneous application of a z gradient and of a frequency-swept adiabatic inversion pulse, as shown in Figure 1 A. The z gradient G_e creates a position-dependent addition to the resonance frequencies of the spins equal to $\gamma G_e z$. The action of the linearly swept π pulse covering all spins over a span L can be approximated as an instantaneous inversion of the spins at a particular z, occurring whenever their spatial + spectral resonance frequencies match the offset of the chirped radio frequency (RF). Therefore, as the frequency-swept pulse is applied, it inverts the spins' magnetizations starting at one end of the sample (e.g. at $\approx +L/2$) and continues to do so along the length of the sample until reaching $z \approx -L/2$. As soon as spins are inverted, however, they begin to recover back to their equilibrium M_0 magnetizations. This in effect can map every site's T_1 IR profile along the length of the sample; given that the swept RF pulse imposes on a priori known relation between position and inversion time, one can then recover the individual IR profiles by reading out the ensuing spatial profiles in a shift-resolved fashion. Such readout can be carried out in a single shot using an EPSI acquisition,[27] of the kind shown in brackets at the end of the sequence in Figure 1 A. This begins with a π/2 pulse putting all the sites' magnetizations in the xy plane, and a pre-winding

gradient that prepares the signal for detection. During the course of the ensuing oscillating train of acquisition gradients G_a, spins with a chemical shift Ω_2 and at a position z precess in the transverse plane, giving rise to a signal of as shown in Equation (1):

$$s(z, \Omega_2) \propto e^{i[k(t_2)z + \Omega_2 t_2]} \qquad (1)$$

where $k(t_2) = \int_0^{t_2} G_a(t')dt'$ is a wavenumber describing the acquisition gradient's action following the π/2 excitation pulse. The overall sample's signal equals the sum of the contributions from all sites over the entire length of the sample [Eq. (2)]:

$$S(k, t_2) \propto \int_{-L/2}^{+L/2} dz \int_{\text{all sites}} d\Omega_2 M_+(\Omega_2, z) e^{i[k(t_2)z + \Omega_2 t_2]} \qquad (2)$$

where $M_+(\Omega_2, z) M_0^{\Omega_2} \left[1 - 2e^{-R_1^{\Omega_2}(z - z_0)} \right]$ is the profile of a particular site's magnetization for $t_2 = 0$, depending on its rate of longitudinal relaxation $R_1^{\Omega_2}$ and possessing its shortest (in principle null) recovery time at $z_0 \approx L/2$. It is apparent that the signal in k-t_2 space is the Fourier conjugate of the shift-resolved distribution of the various sites' magnetizations along z. The desired IR maps should therefore become available by 2D Fourier transform of the data, following their suitable rearrangement in the 2D k-t_2 space. Proper line shapes, however, would only become available if the $k(t_2) = 0$ signal is fully and symmetrically sampled. Ensuring this is the purpose of the preliminary gradient that shifts the imaging echoes to the middle of each ac-

quisition window (a bipolar gradient with a refocusing pulse in its center may be used instead of this preliminary gradient, to remove first-order phase distortions in situations where these may affect spectral quality/phasing). Suitable data processing according to the recipes for EPSI, involving data rearrangement, weighting and 2D FT, leads to the shift-resolved IR curves being sought; an important factor in recovering faithful T_1 recovery estimates includes mapping the NMR coil's sensitivity profile, as described elsewhere.[33]

Materials: All spectral results described in this work were obtained on a Varian 600 MHz VNMRS spectrometer equipped with a multi-resonance inverse gradient probehead. The experiments were carried out at 24 °C. Although a triple-axis-gradient set was available only, the longitudinal z axis, endowed with the strongest field gradients and associated to the longest spatial dimensions, was used to spatially encode the 2D T_1/shift NMR correlations. For the UF-IR sequence, a gradient field strength of 0.5 G cm^{-1} was used to spatially encode longitudinal relaxation and ± 10 G cm^{-1} gradients were used for the EPSI-type acquisition with typical switching times of 10 µs. A 1 s WURST-40 adiabatic inversion pulse with a bandwidth of 4.785 kHz was used to invert sample magnetization. In order to minimize artifacts a 1 s, ~0.1 kHz presaturation pulse was applied on the HDO resonance prior to execution of the sequence; a sinc frequency selective pulse followed by a 5 ms purge gradient (17 G cm^{-1}) was also applied after the spatial encoding to minimize artifacts arising from HDO that relaxed back to equilibrium during the spatial encoding of longitudinal relaxation.

These UF-IR experiments were complemented by MA-IR acquisitions (Figure 1 B). Here, Gaussian pulses with a 1 % truncation level were used for slice-selective excitation and refocusing. The frequency offsets for the selective pulses were varied from 51.1 to −51.1 kHz in increments of ~11.4 kHz and they were applied synchronously with a 16 G cm^{-1} magnetic field gradient. To ensure complete inversion of the sample magnetization in these MA-IR experiments, a short (2 ms) frequency-swept adiabatic inversion pulse was applied. Ten acquisition periods were used to sample the IR curves, with each acquisition period being 1.5 s long, totaling 15 s. A recycle delay of 30 s was employed to ensure that the magnetization of all the slices fully recovered to equilibrium (the longest T_1 was ~6 s). Traditional IR experiments (Figure 1 C) were also applied to the systems investigated.
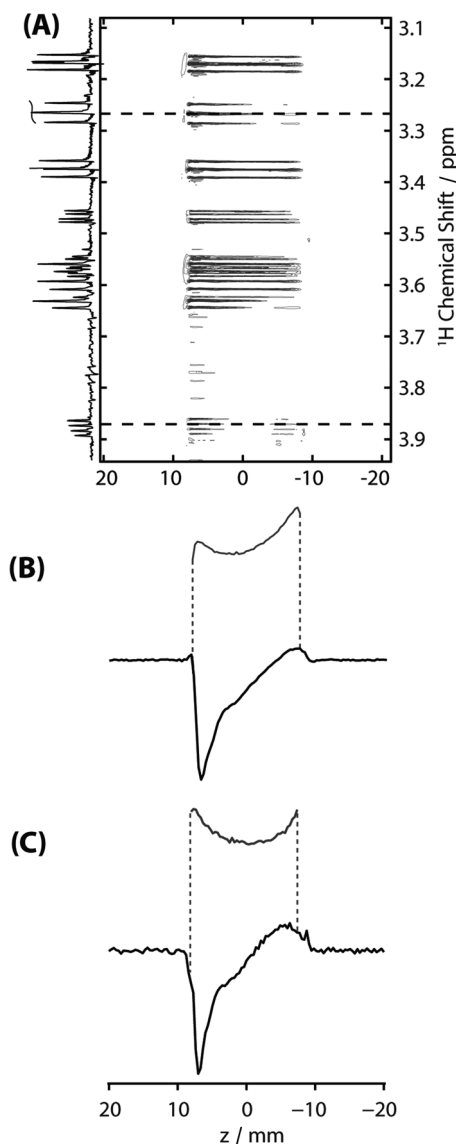
The usefulness of the UF-IR and MA-IR methods to monitor real-time transformations, was explored by analyzing the nature of the xylose–borate reaction. Further insight regarding the connectivity of the various species intervening in this mixture was obtained using conventional and ultrafast (Figure 1 D) 2D TOCSY NMR. These spectra are represented in magnitude mode.

A variety of Matlab 8.0 software programs (The Mathworks) were written for processing the data. All chemicals and solvents were obtained from Aldrich and used as purchased.
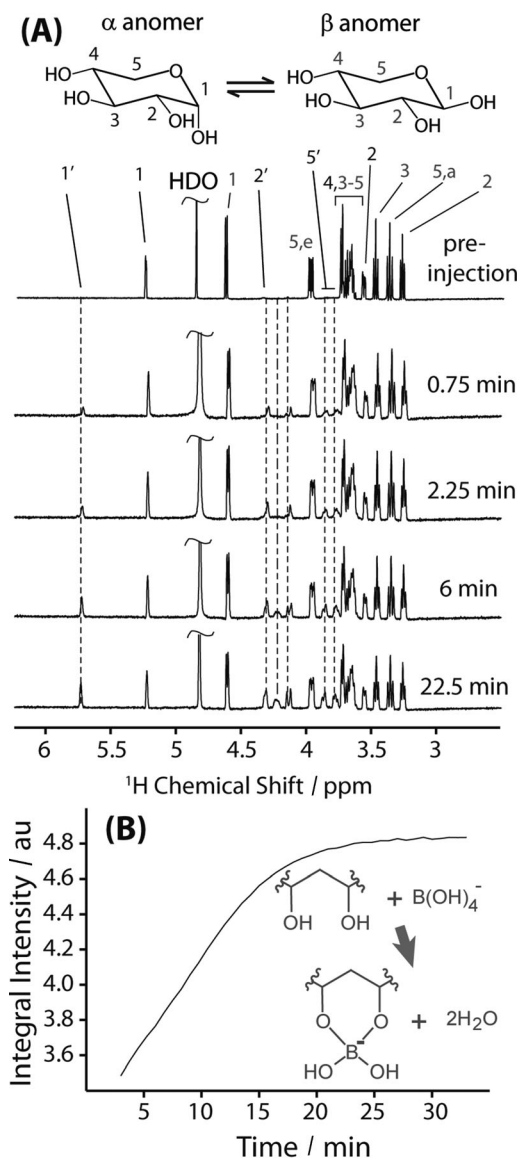
2. Results and Discussion

The Ultrafast Inversion-Recovery Sequence

To test the performance of the UF-IR method just outlined, the IR behavior of 100 mm D-xylose dissolved in D$_2$O was monitored. Figure 2 A illustrates representative results of these tests, shown as a 2D plot displaying the recovery contours observed for each chemical site as a function of position corresponding to a Δ_{IR} of 100 ms. Two slices show the spatial variation in transverse magnetization induced by longitudinal relaxation at

Figure 2. A) UF-IR spectrum acquired on 100 mm D-xylose dissolved in D$_2$O; illustrating contours of the spins' recovery as a function of position as well as the 1D spectrum emerging of the data at $\Delta_{IR} \approx 100$ ms. These data arise from the sequence shown in Figure 1 A, after processing its signal in an EPSI-like fashion. Slices taken at $\delta \sim 3.3$ ppm (B) and $\delta \sim 3.9$ ppm (C) illustrate the variation of magnetization along the length of the sample set up by an adiabatic inversion pulse applied synchronously with a magnetic field gradient. Shown in gray are profiles arising from the same sites after full recovery; these are needed as reference for an accurate reconstruction of the IR curves.

chemical shifts of $\delta \sim 3.3$ and ~ 3.9 ppm (Figure 2B, C). IR curves can be reconstructed from these spatial profiles, by normalization against a priori known coil-sensitivity profiles (gray curves in Figure 2B, C). The peaks shown in Figure 2 arise from the axial and equatorial β_5-proton sites of D-xylose ($\beta_{5,a}$ and $\beta_{5,e}$, see Figure 3A), which exhibit faster relaxation times due
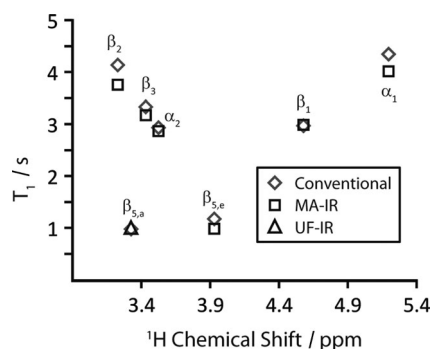
to their proximity to each other. Note that the individual sites and their splitting patterns are resolved in the 2D plot after EPSI processing. This illustrates some of the advantages of the UF-IR technique, including its ability to provide single-shot longitudinal relaxation measurements with high time resolution and without sacrificing spectral resolution. This feature would not be available if the MA-IR experiment would be used to analyze peaks like these ones, for which T_1 and T_2 values are comparable. On the other hand, the range of relaxation times that can be measured by UF-IR may be limited by the length of time for which a suitable encoding gradient can be applied, or compromised if dealing with sites with very different relaxation times.

At the edges of the sample images shown in Figure 2B and C, at $\sim \pm 9$ mm, anomalous decreases in signal intensities are observed. These effects—which are often seen in gradient shimming experiments—reflect variations in the main magnetic field homogeneity throughout the sample, non-linearities in the applied field gradient as well as RF inhomogeneities throughout the length of the excitation/detection coil. Of all these the inhomogeneous detection factor is probably most important, as slight deviations in the RF pulse delivered throughout the adiabatic sweep or in B_0's ideal profile, are not expected to affect significantly a signal's strength. In order to account for all these variations, the points along an UF-IR curve need to be divided by a reference image (shown in gray in Figure 2B, C). Note that such normalizations were also required for processing the MA-IR and the single-scan DOSY data.[26,33]

It should be noted that if seeking to measure very short T_1s, shorter chirp pulses should be used, leading to a more finely sample IR curve. However, if necessary to measure both longer and shorter T_1s simultaneously (for instance ≥ 1 s and ≤ 0.1 s), a high resolution and extended dynamic range in the z/T_{IR} dimension is required. This in turn may translate in a need for a more extended sampling in EPSI's k-dimension, demanding a concomitant increase in either the associated gradient strength or in the dwell times along the t_2 dimension. The latter choice may bring a decrease in the spectral width of the corresponding f_2 dimension, which may make it necessary to account for aliasing artifacts.[27] Furthermore, if there are a wide range of T_1s associated with the resonances of UF-IR spectrum, the user might be required to use a long WURST-40 pulse and gradient, which may be associated with hardware limitations.[26]

A comparison of the relaxation time measurements thus emerging from single-scan and from conventional IR methods is given in Figure 4. There is a close correspondence between the T_1s measured by single-scan and conventional IR techniques for all the sites except the $\beta_{5,e}$ site, and the results do not differ by more than 10%. Note that in the UF-IR experiment the encoding gradient was applied for a second, limiting the range of T_1s observable using this single-scan technique to ≤ 1 s. The relatively larger disagreement between conventional IR and MA-IR for the $\beta_{5,e}$ site (16%) may be reflecting cross-correlations between the dipolar- and chemical-shift-mediated T_1 relaxation mechanisms, leading to relaxation behavior which is

Figure 3. Overview of the xylose–borate reaction. A) Series of 1D ^{1}H NMR spectra of the D-xylose solution/xylose-borate reaction mixture as a function of time (shown on the right side of each spectrum) after sodium borate injection. The protons of uncomplexed D-xylose are assigned as labeled on the α (gray) and β (black) anomeric forms shown at the top; "e" refers to an equatorial proton and "a" refers to an axial proton (assignments taken from ref. [48]). Primed numbers correspond to xylose peaks in the 1:1 xylose-borate complex (assigned by TOCSY and IR spectra) and unprimed peaks correspond to uncomplexed xylose. Note that in the text, the anomeric form of the resonance is referenced with a Greek letter and the number is indicated with a subscript (e.g. α_1 indicates the anomeric peak of the α anomer of xylose). Lines with equal dashes indicate new peaks associated with the 1:1 borate:xylose complex and the line with unequal dashes indicates a new peak associated with the 1:2 borate:xylose complex. B) Integral intensity of the HDO peak as a function of time after the injection of sodium borate. The inset shows the mechanism of borate-diol interaction.[43]

Special Section: NMR Spectroscopy

Figure 4. T_1 values derived from fits to the IR curves obtained from conventional IR (gray diamonds), MA-IR (black squares), and UF-IR (black triangles) plotted against chemical shift. The markers are labeled with resonance assignments (given in Figure 3). Note that only T_1s ≤ 1 can be reliably observed using UF-IR because the encoding gradient was applied for no longer than one second.
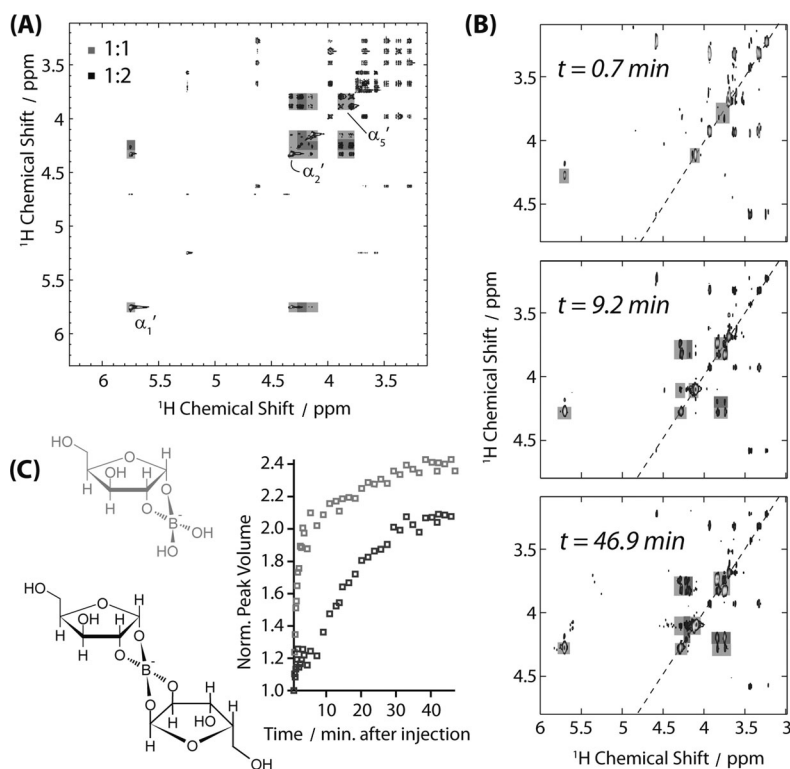
not strictly monoexponential. Then, as for the MA-IR experiment larger Δ_{IR} values are sampled on the IR curve, slowly relaxing components exert a larger influence on the T_1 fit value.

Monitoring Xylose–Borate Reaction Kinetics with the UF-IR and 2D TOCSY Techniques

In order to explore the ability of these single-shot IR methods to monitor real-time chemical changes, they were applied to study the xylose–borate reaction. This process has been investigated by a number of means,[34–36] including NMR. Boronic acids bind with high affinity to compounds containing diol moieties through reversible ester formation.[37]

This tight binding allows for the use of boronic acids and their derivatives in the construction of sensors for saccharides,[28,29,38,39] as affinity ligands for the separation of carbohydrates and glycoproteins,[30,31,40] and as antibody mimics for cell-surface polysaccharides.[41,42] Shown in Figure 3A is a time series of ^{1}H NMR spectra collected upon adding 100 μL of 50 mM sodium borate to a 600 μL solution of 100 mM D-xylose under basic (pD > 10) conditions. Both of these solutions were prepared in D_2O, and the reaction was triggered by injecting the sodium borate into

D-xylose with a custom-made apparatus. D-Xylose has two interconverting pyranose (six-membered ring) and furanose (five-membered ring) forms; the pyranose forms are more stable than the furanose ones due to their reduced intra-ring strains; peaks in the spectrum of pure D-xylose (Figure 3A, top trace) are therefore assigned to these pyranose forms. As the reaction proceeds water is produced, as is evidenced by the increasing intensity of the HDO peak (Figure 3B) and, as would be predicted, on the basis of the borate anion's interaction with polyols.[43] To interpret the remaining spectral changes it is worth remembering that: 1) it is known that the borate anion only interacts with the α anomers of xylose;[36] 2) there is some evidence that it interacts with the furanose form of D-xylose;[34,44] and 3) it was recently shown that under certain conditions, some simple sugars associate with the borate anion while in their pyranose form.[45] Because of the proximity of the α_5' protons to each other in the borate-xylose complex, they exhibit short T_1s and may be easily identified with inversion recovery methods. If the borate–xylose complex is exclusively associated with D-xylose's furanose forms, two resonances for the diastereotopic α_5 protons can be expected at
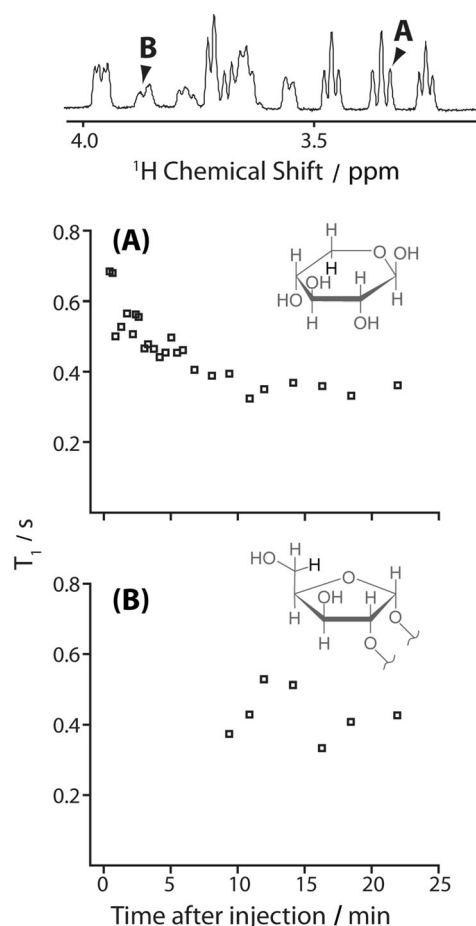

Figure 5. A) Conventional TOCSY experiment acquired on the equilibrated reaction product. Peaks uniquely assigned to the 1:2 borate–xylose complex are shown against a dark gray background and peaks associated with the 1:1 (and possibly 1:2) borate–xylose complex(es) are shown against a light gray background. A 40 ms DIPSI mixing sequence was used and 1024 points were acquired in the t_1 dimension with a sw$_1$ of 2500 Hz. B) Representative ultrafast TOCSY spectra acquired 0.7, 9.2, and 46.9 min after the injection of borate. These data were collected using the sequence in Figure 1D with chirped pulses spanning 79 kHz; $G_e = 10$ G cm^{-1}; $t_1^{max}/2 = 17.5$ ms; $G_a = 14.76$ G cm^{-1}; $T_a = 542$ μs; $N_2 = 180$. A bipolar purge gradient (G_p) of 25 G cm^{-1} was applied for 1.1 ms prior to acquisition and, in order to ensure all peaks fell within the f$_1$ spectral window, an extra gradient (k-shift in Figure 1D) was applied at -G_e for 3.15 ms. Data were sampled every 2 μs and each data set was subject to a suitable shearing transform and zero filling along both dimensions before t_2 Fourier transformation. A 40 ms long DIPSI-2 mixing pattern was used. C) The reaction products are shown to the left. Shown to the right (in light gray) is the sum of peak volumes associated with the 1:1 and 1:2 borate-xylose peaks (shown is a green highlight in panels A and B), and (in dark gray) the sum of peak volumes uniquely associated with the 1:2 borate-xylose peaks.

$\delta \sim 3.65$ and ~ 3.80 ppm; this is observed, for example, in the ¹H NMR spectrum of similar D-xylofuranose compounds such, as 1,2-cyclohexylidene-3-O-tosyl-α-D-xylofuranose.[46] On the other hand, if the borate anion complexes with the pyranose form of D-xylose, one would expect to observe peaks corresponding to the α_5 axial and equatorial protons, which, in the case of 1,4-anhydro-2,3-di-O-benzyl-α-D-xylopyranose, appear at $\delta = 3.39$ and 4.06 ppm (separated by more than $\delta = 0.6$ ppm).[47] Given the fact that two equal intensity peaks with short T_1 values appear initially at $\delta = 3.74$ and 3.84 ppm, separated by less than $\delta = 0.2$ ppm (Figure 3 A), the borate-xylose complexes formed are most likely associated with the furanose form of D-xylose. This result is in agreement with the one reported by Chapelle and Verchere.[34]

The borate anion associates with a maximum of two diol moieties.[43] Early in the reaction a set of new ¹H NMR peaks appear simultaneously, as indicated by the lines with equal-length dashes in Figure 3 A. These are probably associated with a 1:1 borate–xylose complex; it is unlikely that, early on in the reaction, the borate ion forms a complex with two D-xylose molecules simultaneously. The results of Pepi et al. suggest that the borate anion associates with D-xylose at the O1 and O2 oxygens and that the tridentate boronate ester structure, in which the borate anion associates with the O1, O3, and O5 oxygens, is not formed.[45] Further along in the time course of the reaction a new peak appears (shown by the line with unequal length dashes in Figure 3 A) indicating the presence of a new species and strongly suggesting the formation of a 1:2 borate–xylose complex.[34] To get further insight into this possibility, TOCSY experiments on the equilibrated reaction mixture were recorded. This conventional 2D spectrum suggests the presence of at least two species, since at a mixing time of 40 ms, resonances appear to be separated into two groups with no common cross-peaks evident (Figure 5 A). This, however, could be misleading, as some of the peaks in the various borate–xylose complexes formed at the conclusion of the reaction may overlap. One possible way to alleviate this problem is to follow the cross-peaks arising in the 2D trace in real time, using the ultrafast TOCSY sequence presented in Figure 1 D. Representative ultrafast TOCSY spectra are shown 0.7, 9.2, and 46.9 min after the injection of borate, in Figure 5 B. These traces allow us to distinguish peaks that are uniquely identified with the 1:1 borate–xylose complex, from those associated with either the 1:2 complex or from both the 1:1 and 1:2 complexes (identified with equal and unequal length dashed lines in Figure 3 A, respectively). These data also show that the α_1' peak (Figure 5 A) shares a cross peak with the 1:2 peak as well as with the 1:1 borate–xylose complex, and is not associated with a single species in the reaction mixture. Nevertheless, when the co-added peak volumes of all the peaks associated with the 1:1 borate–xylose complex are compared with the co-added peak volumes of all the peaks uniquely assigned to the 1:2 borate–xylose complex, it is clear that a 1:1 borate–xylose species is formed first, and that further along in the course of the reaction a 1:2 borate–xylose species is formed subsequently; these data are summar-

ized by the light gray and dark gray data points shown in the time progression of Figure 5 C.

The use of UF-IR to track the reaction of D-xylose with the borate anion could also be helpful to establish the temporal precedence with which new peaks appear in the xylose–borate mixture. Figure 6 A shows the variation of the D-xylose monomer $\beta_{5,a}$ proton's longitudinal relaxation as a function of time, as monitored by UF-IR. Changes in the magnetic susceptibility of the sample occur upon mixing the reactants. These susceptibility changes create magnetic field inhomogeneity, which manifests as a variation in the resonance frequency of the spins throughout the length of the sample and as a "warping" of the sample images. However, this effect was easily corrected for by using a reference (unwarped) sample image.[49] Note the correspondence between the decrease in this proton's T_1 and the formation of the borate complex; an increase in molecular weight, plus the higher concentration of solvent protons as the reaction proceeds, probably lead to this decrease in the T_1 for the ¹H nuclei associated with the D-xylose molecules and the borate-xylose complexes. This finding also highlights the

Figure 6. Variation of T_1 as a function of time after the injection of borate, monitored using UF-IR. The peaks for which T_1s are provided are identified in the ¹H spectrum given above the plots. A) Variation of T_1 as a function of time for the axial β_5 hydrogen of uncomplexed D-xylose (depicted in black in the inset). B) Variation of T_1 as a function of time for the 1:1 xylose-borate complex peak at $\delta = 3.84$ ppm (depicted in black in the inset).

sensitivity of UF-IR to changes in the nuclear environment, such as changes in molecular dynamics or in the location of nearby protons that serve as relaxation sinks. The T_1 variation of the peak at $\delta = 3.84$ ppm (second furthest upfield among the new peaks) as a function of the time after the reaction is initiated, is shown in Figure 6 B. This peak is associated with the formation of the 1:1 borate–xylose complex. Because an adequate signal-to-noise ratio to measure the T_1 of the new peak is only available later in the course of the reaction, when the increased density of the ^{1}H nucleus already exerts an effect on the T_1s of all the resonances, a significant change in this peak's T_1 is not observed.

In order to investigate the trend of a decrease in T_1 associated with the reaction's progression, the xylose–borate reaction was monitored with MA-IR. Figure 7 A shows a series of T_1s obtained using MA-IR for the α_1 proton of uncomplexed D-xylose, which may be compared with the T_1 obtained using MA-IR on uncomplexed D-xylose prior to the reaction's initialization (indicated with a dashed horizontal line). In order to measure these protons' T_1s, a longer recycle delay ($\sim 5 \times 6$ s $= 30$ s) had to be utilized and furthermore, the acquisition of 1D ^{1}H spectra for ten slices, each with an acquisition time of 1.5 s, took 15 s. A decrease in T_1 relative to the α_1 proton's T_1 prior to reaction initialization can be seen, however T_1 values remain relatively constant after the reaction initialization. Although the fact that the reaction is proceeding while the T_1 of these protons is being measured (a process which lasts 15 s) complicates interpretation of these T_1 values, it is nevertheless clear that after the T_1 values stabilize, they remain shorter than the T_1 value observed prior to reaction initialization. Figure 7 B shows a series of T_1s obtained using MA-IR for the β_1 proton of uncomplexed D-xylose, which is again shorter than the T_1 obtained for the β_1 proton prior to reaction initialization (horizontal dashed line). In Figure 7 C, T_1 values associated α_1' resonance of the borate-xylose complex are plotted. Notably, the T_1s observed for this peak are ~ 0.5 s shorter than those observed for the α_1 resonance, which illustrates the feasibility of distinguishing different molecular species, such as uncomplexed D-xylose and the borate-xylose complex, on the basis of T_1. Even for challenging, broad resonances, such as α_2', MA-IR can be used to extract T_1s in real time, as shown in Figure 7 D.
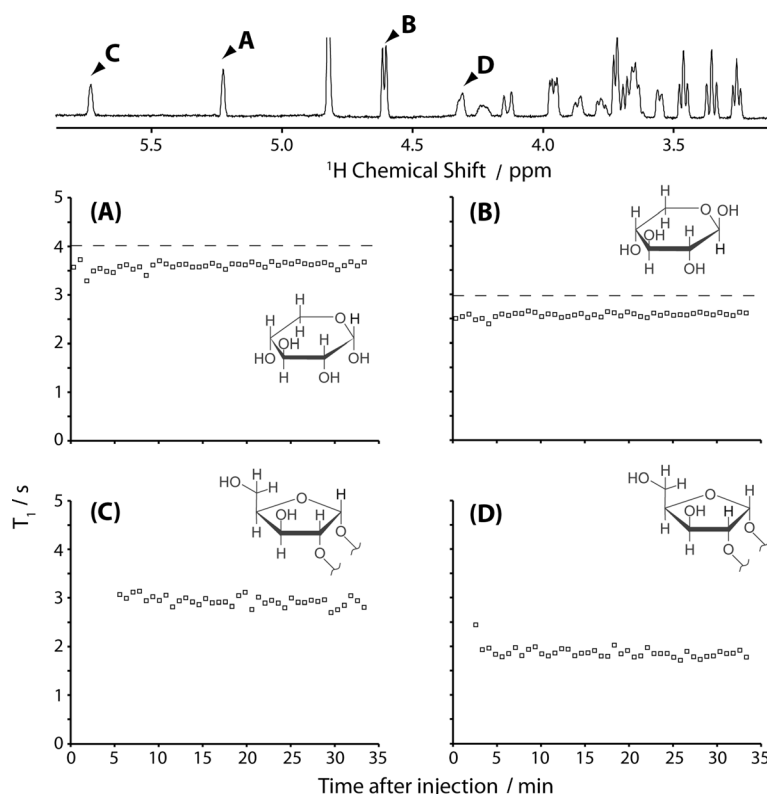
3. Conclusions

Information regarding the longitudinal relaxation of NMR-active nuclei can yield valuable insights into the flexibility of molecules. Of particular importance would be new methods to monitor the changes as complexation and aggregation occur in real time when molecules undergo reactions or biophysical functions. Here, a new ultrafast method to monitor the flexibility changes occurring in molecules in real time is developed and its use is demonstrated on the reaction of D-xylose with borate. Results obtained by other ultrafast 2D spectroscopic methods complement well the insight obtained from IR methods. For spins exhibiting a range from long to short longitudinal relaxation values, UF-IR may be supplemented with the MA-IR technique. Using the combined methods, changes in relaxation parameters associated with a uni-directional reaction can be investigated for an array of timescales. Further efforts are under way to investigate similar phenomena in pathological and non-pathological biological processes.

Figure 7. Variation of T_1 as a function of time after the injection of borate, monitored using MA-IR. The peaks for which T_1s are provided are identified in the ^{1}H spectrum given above the plots. A) The variation of T_1 as a function of time for the α_1 hydrogen of uncomplexed D-xylose, B) for the β_1 hydrogen of uncomplexed D-xylose, C) for the α_1' hydrogen of the borate-xylose complex, and D) for the α_2' hydrogen of the borate-xylose complex. The associated protons are depicted in insets in black.

[1] K. A. Henzler-Wildman, M. Lei, V. Thai, S. J. Kerns, M. Karplus, D. Kern, *Nature* **2007**, *450*, 913 – 916.
[2] A. G. Palmer, J. Williams, A. McDermott, *J. Phys. Chem.* **1996**, *100*, 13293 – 13310.
[3] V. Guallar, M. Jacobson, M. McDermott, R. A. Friesner, *J. Mol. Biol.* **2004**, *337*, 227 – 239.
[4] J. C. Williams, A. E. McDermott, *Biochemistry* **1995**, *34*, 8309 – 8319.
[5] L. E. Kay, D. A. Torchia, A. Bax, *Biochemistry* **1989**, *28*, 8972 – 8979.
[6] I. Bertini, C. Luchinat, Y. Niikura, C. Presenti, *Protein* **2000**, *41*, 75 – 85.
[7] J. García de la Torre, M. L. Huertas, B. Carrasco, *J. Magn. Reson.* **2000**, *147*, 138 – 146.
[8] R. Ghose, D. Fushman, D. Cowburn, *J. Magn. Reson.* **2001**, *149*, 204 – 217.
[9] R. Soong, J. R. Brender, P. M. Macdonald, A. Ramamoorthy, *J. Am. Chem. Soc.* **2009**, *131*, 7079 – 7085.
[10] R. Ishima, D. A. Torchia, *Nat. Struct. Mol. Biol.* **2000**, *7*, 740 – 743.
[11] J. Cavanagh, M. Akke, *Nat. Struct. Mol. Biol.* **2000**, *7*, 11 – 13.
[12] J. D. Forman-Kay, *Nat. Struct. Mol. Biol.* **1999**, *6*, 1086 – 1087.
[13] M. Akke, R. Bruschweiler, A. G. Palmer, *J. Am. Chem. Soc.* **1993**, *115*, 9832 – 9833.
[14] Z. Li, S. Raychaudhuri, A. J. Wand, *Protein Sci.* **1996**, *5*, 2647 – 2650.
[15] D. Yang, L. E. Kay, *J. Mol. Biol.* **1996**, *263*, 369 – 382.
[16] L. Zidek, M. V. Novotny, M. J. Stone, *Nat. Struct. Biol.* **1999**, *6*, 1118 – 1121.
[17] A. L. Lee, S. A. Kinnear, A. J. Wand, *Nat. Struct. Biol.* **2000**, *7*, 72 – 77.
[18] C. Bracken, P. A. Carr, J. Cavanagh, A. G. Palmer, *J. Mol. Biol.* **1999**, *285*, 2133 – 2146.
[19] D. C. Look, D. R. Locker, *Rev. Sci. Instrum.* **1970**, *41*, 250 – 251.
[20] I. Kay, R. M. Henkelman, *Magn. Reson. Med.* **1991**, *22*, 414 – 424.
[21] P. Gowland, P. Mansfield, *Magn. Reson. Med.* **1993**, *30*, 351 – 354.
[22] C. A. McKenziea, F. S. Pratoa, R. E. Thornhill, D. J. Drosta, *Magn. Reson. Imaging* **2000**, *18*, 129 – 138.
[23] R. Bhattacharyya, A. Kumar, *Chem. Phys. Lett.* **2004**, *383*, 99 – 103.
[24] R. Kaptein, K. Dijkstra, C. E. Tarr, *J. Magn. Reson.* **1976**, *24*, 295 – 300.
[25] I. J. Day, J. C. Mitchell, M. J. Snowden, A. L. Davis, *J. Magn. Res.* **2007**, *187*, 216 – 224.
[26] N. M. Loening, M. J. Thrippleton, J. Keeler, R. G. Griffin, *J. Magn. Reson.* **2003**, *164*, 321 – 328.
[27] P. Mansfield, *Magn. Reson. Med.* **1984**, *1*, 370 – 386.
[28] T. D. James, K. R. A. S. Sandanayake, R. Iguchi, S. Shinkai, *J. Am. Chem. Soc.* **1995**, *117*, 8982 – 8987.
[29] T. D. James, K. R. A. S. Sandanayake, S. Shinkai, *Angew. Chem.* **1996**, *108*, 2038 – 2050; *Angew. Chem. Int. Ed. Engl.* **1996**, *35*, 1910 – 1922.
[30] X.-C. Liu, J. L. Hubbard, W. H. Scouten, *J. Organomet. Chem.* **1995**, *493*, 91 – 94.
[31] V. Adamek, X.-C. Liu, Y. A. Zhang, K. Adamkova, W. H. Scouten, *J. Chromatogr.* **1992**, *625*, 91 – 99.
[32] Y. Shrot, B. Shapira, L. Frydman, *J. Magn. Reson.* **2004**, *171*, 163 – 170.
[33] Y. Shrot, L. Frydman, *J. Magn. Reson.* **2008**, *195*, 226 – 231.
[34] S. Chapelle, J.-F. Verchere, *Tetrahedron* **1988**, *44*, 4469 – 4482.
[35] J.-F. Verchere, M. Hlaibi, *Polyhedron* **1987**, *6*, 1415 – 1420.
[36] L. Ciobanu, D. A. Jayawickrama, X. Zhang, A. G. Webb, J. V. Sweedler, *Angew. Chem.* **2003**, *115*, 4817 – 4820; *Angew. Chem. Int. Ed.* **2003**, *42*, 4669 – 4672.
[37] G. Springsteen, B. Wang, *Tetrahedron* **2002**, *58*, 5291 – 5300.
[38] W. Yang, H. He, D. G. Drueckhammer, *Angew. Chem.* **2001**, *113*, 1764 – 1768; *Angew. Chem. Int. Ed.* **2001**, *40*, 1714 – 1718.
[39] S. Arimori, L. I. Bosch, C. J. Ward, T. D. James, *Tetrahedron Lett.* **2001**, *42*, 4553 – 4555.
[40] P. R. Westmark, L. S. Valencia, B. D. Smith, *J. Chromatogr. A* **1994**, *664*, 123 – 128.
[41] A. Sugasaki, K. Sugiyasu, M. Ikeda, M. Takeuchi, S. Shinkai, *J. Am. Chem. Soc.* **2001**, *123*, 10239 – 10244.
[42] W. Yang, S. Gao, X. Gao, V. V. R. Karnati, W. Ni, B. Wang, W. B. Hooks, J. Carson, B. Weston, *Bioorg. Med. Chem. Lett.* **2002**, *12*, 2175 – 2177.
[43] S. W. Sinton, *Macromolecules* **1987**, *20*, 2430 – 2441.
[44] H. Eggert, J. Frederiksen, C. Morin, J. C. Norrild, *J. Org. Chem.* **1999**, *64*, 3846 – 3852.
[45] F. Pepi, S. Garzoli, A. Tata, P. Giacomello, *Int. J. Mass Spectrom.* **2010**, *289*, 76 – 83.
[46] P. A. Hadžić, N. S. Vukojević, *J. Serb. Chem. Soc.* **2001**, *66*, 289 – 295.
[47] T. Uryu, J. Yamanouchi, S. Hayashi, H. Tamaki, K. Matsuzaki, *Macromolecules* **1983**, *16*, 320 – 326.
[48] A. J. Benesi, C. J. Falzone, S. Banerjee, G. K. Farber, *Carbohydr. Res.* **1994**, *258*, 27 – 33.
[49] P. Irrazabal, C. H. Meyer, D. G. Nishimura, A. Macovski, *Magn. Reson. Med.* **1996**, *35*, 278 – 282.

Special Section: NMR Spectroscopy